Effects of Side-Chain Charges on α-Helix Stability in C-Peptide of Ribonuclease A Studied by Multicanonical Algorithm

Ulrich H. E. Hansmann† and Yuko Okamoto*

Department of Theoretical Studies, Institute for Molecular Science, Okazaki, Aichi 444-8585, Japan

Received: August 25, 1998; In Final Form: December 10, 1998

We have performed multicanonical Monte Carlo simulations of C-peptide of ribonuclease A. Three analogues of the peptide with charged and neutral side chains were used to study the role of side-chain charges in the stability of the observed α-helix. Two dielectric functions, distance-dependent and constant, are considered to study the effects of solvent contributions. The results are found to be in accord with the implications of CD and NMR experiments of C-peptide where it was found that this peptide has high α-helix content in aqueous solution and that the removal of the side-chain charge of Glu-9$^-$ enhances helix formation. The lowest-energy conformation obtained by our simulations has an α-helix from Ala-4 to Gln-11 in complete agreement with the corresponding structure deduced from an X-ray crystallography experiment of ribonuclease A. The salt bridge between the side chains of Glu-2$^-$ and Arg-10$^+$, which is known to exist from both NMR and X-ray experiments, is formed only when the side chains are properly charged. Its formation is greatly enhanced when the solvation effects are taken into account.

Introduction

The C-peptide, residues 1−13 of ribonuclease A, is known by CD and NMR experiments[1,2] to have significant α-helix formation in aqueous solution at temperatures near 0 °C and to form the characteristic salt bridge between Glu-2$^-$ and Arg-10$^+$ that is found in the native structure of ribonuclease A.[3] The CD experiment of C-peptide showed that the side-chain charges of residues Glu-2$^-$ and His-12$^+$ play an important role in the stability of the α-helix, while the removal of the side-chain charge of Glu-9$^-$ enhances helix formation.[1]

A previous simulation work[4] by Monte Carlo simulated annealing[5] confirmed the α-helix formation and the importance of the electrostatic interactions of the above three side chains for the stability of the helix. The simulation was performed in gas phase, however, and it failed in obtaining the characteristic salt bridge between Glu-2$^-$ and Arg-10$^+$.

In this article, we study the α-helix stability of C-peptide and its relation to side-chain electrostatic interactions in more detail. For this purpose, we employ a more sophisticated technique, the *multicanonical algorithm*,[6,7] which belongs to the class of *generalized-ensemble methods* (for a discussion and comparison of these algorithms, see, for instance, ref 8). This method was introduced to the protein folding problem a few years ago,[9] and the effectiveness of the method has been established for oligopeptide systems.[10,11] In our case, the utilization of the novel method proved crucial and allowed us to overcome the multiple-minima problem that is responsible for the very long equilibrization time required by conventional methods. Sampling a wide range of configuration space, we were able to study the formation of α-helix structures in C-peptide in much greater detail than was possible in previous work.[4] As a result, we found that the lowest-energy conformation obtained by the simulation has an α-helix from Ala-4 to Gln-11 in complete agreement with the corresponding structure deduced from an X-ray crystallographic experiment of the whole ribonuclease A.[3] It is shown that the characteristic salt bridge between Glu-2$^-$ and Arg-10$^+$, which is known to exist both in the NMR experiment of C-peptide[2] and in the X-ray experiment of ribonuclease A,[3] is formed with significant probability only when the side chains are properly charged and some solvation effects are included. Preliminary results of the present work were reported elsewhere.[12]

In the following sections we first review our simulation techniques and explain the method of our analyses. We then present the results, compare them with experimental results, and finish with the conclusions.

Methods

Multicanonical Algorithms. While a regular Monte Carlo method[13] generates states according to the canonical distribution, the multicanonical algorithms[6,7] generate states so that a one-dimensional random walk in energy space is realized. Hence, any energy barrier can be overcome, and one can avoid getting trapped in states of energy local minima.

In the "multicanonical ensemble" the probability distribution of energy is *defined* as follows:

$$P_{\mathrm{mu}}(E) \propto n(E)W_{\mathrm{mu}}(E) \equiv \text{constant} \tag{1}$$

The multicanonical weight factor then satisfies

$$W_{\mathrm{mu}}(E) \propto n^{-1}(E) \tag{2}$$

Since this weight factor is not *a priori* known, one has to determine it for each system by a few iterations of trial Monte Carlo simulations. See refs 7, 10, and 11 for details of the method to determine the multicanonical weight factor $W_{mu}(E)$.

The advantage of multicanonical algorithms (and generalized-ensemble methods in general) lies in the fact that it allows one

† E-mail: hansmann@mtu.edu. Present address: Department of Physics, Michigan Technological University, Houghton, MI 49931-1295.

* To whom correspondence should be addressed. E-mail: okamotoy@ims.ac.jp.

10.1021/jp983479e CCC: $18.00
Published on Web 02/06/1999

to sample a wide range of configuration space and overcome the multiple-minima problem that is responsible for the very long equilibrization time required by conventional methods. From a single simulation run, it thus enables one to obtain not only the lowest-energy conformation but also any thermodynamic quantity over a wide range of temperatures $T = 1/k_B\beta$.[6,9] The latter is accomplished by the use of the reweighting techniques,[14] which allows one to calculate the expectation value of a physical quantity A at temperature T by

$$\langle A \rangle_T = \frac{\int \mathrm{d}x\, A(x)\, W_{\mathrm{mu}}^{-1}(E(x))\mathrm{e}^{-\beta E(x)}}{\int \mathrm{d}x\, W_{\mathrm{mu}}^{-1}(E(x))\mathrm{e}^{-\beta E(x)}} \tag{3}$$

where x stands for configurations.

Potential Energy Function. In this work, we used three analogues of C-peptide in order to study the importance for α-helix stability due to the electrostatic interactions of the side-chain charges of residues Glu-2, Glu-9, and His-12. The amino acid sequences of these analogues are summarized in Table 1. These choices are made because the experimental results suggested that the charges of Glu-2 and His-12 are important for the stability of the α-helix structure, while the removal of the charge of Glu-9 enhances the helix formation.[1,2] Although, in experiments, the charges of Glu-2$^-$, Glu-9$^-$, and His-12$^+$ are removed by replacing them by Ala-2, Leu-9, and Ala-12, respectively,[1,2] here we just replace them by their neutral counterparts for simplicity, i.e., by neutral Glu-2, Glu-9, and His-12, respectively. Since the charges at peptide termini are known to reduce helix content,[15,16] we removed them by taking a neutral NH_2- group at the N-terminus and a neutral $-$COOH group at the C-terminus.

The potential energy function that we used is given by the sum of the electrostatic term, 12-6 Lennard-Jones term, and hydrogen-bond term for all pairs of atoms in the peptide together with the torsion term for all torsion angles:

$$E_{\mathrm{tot}} = E_{\mathrm{C}} + E_{\mathrm{LJ}} + E_{\mathrm{HB}} + E_{\mathrm{T}}$$

$$E_{\mathrm{C}} = \sum_{(i,j)} \frac{332 q_i q_j}{\epsilon r_{ij}}$$

$$E_{\mathrm{LJ}} = \sum_{(i,j)} \left(\frac{A_{ij}}{r_{ij}^{12}} - \frac{B_{ij}}{r_{ij}^{6}} \right)$$

$$E_{\mathrm{HB}} = \sum_{(i,j)} \left(\frac{C_{ij}}{r_{ij}^{12}} - \frac{D_{ij}}{r_{ij}^{10}} \right)$$

$$E_{\mathrm{T}} = \sum_{l} U_l (1 \pm \cos(n_l \chi_l)) \tag{4}$$

Here, r_{ij} (in Å) is the distance between atoms i and j, ϵ is the dielectric constant, and χ_l is the torsion angle for the chemical bond l. Bond lengths and bond angles were fixed at experimental values, leaving the dihedral angles ϕ, ψ, and χ as independent variables (the peptide-bond dihedral angles ω were fixed to their common value 180° for simplicity). The energy parameters were adopted from ECEPP/2.[17] A sigmoidal, distance-dependent dielectric function[18] was used to mimic the presence of water. The explicit form of the function we used is given by[19]

$$\epsilon(r) = D - \frac{D-2}{2}[(sr)^2 + 2sr + 2]\mathrm{e}^{-sr} \tag{5}$$

TABLE 1: Amino Acid Sequences of the C-Peptide Analogues Used in the Present Work[a]

	Peptide		
	I	II	III
residue			
1	Lys^+		
2	Glu^-		Glu
3	Thr		
4	Ala		
5	Ala		
6	Ala		
7	Lys^+		
8	Phe		
9	Glu^-	Glu	
10	Arg^+		
11	Gln		
12	His^+		His
13	Met		

[a] Entries for Peptides II and III indicate that the corresponding residues in Peptide I are substituted by those with neutral side chain (and empty entries imply that no change from Peptide I is made for the corresponding residue).

which is a slight modification of the one used in ref 20. Here, we use $s = 0.3$ and $D = 78$. It approaches 2 (the value inside a protein) in the limit the distance r going to zero and 78 (the value for bulk water) in the limit r going to infinity. A constant dielectric function ($\epsilon = 2$) was also used for a comparison with gas-phase simulations. Hereafter, we refer to the simulations with the sigmoidal dielectric function and the constant dielectric function as $\epsilon =$ sig and $\epsilon = 2$, respectively. The computer code KONF90[4] was used. (There are slight differences in conventions between KONF90 and the original version of ECEPP/2; for example, ϕ_1 of KONF90 is equal to $\phi_1 - 180°$ of ECEPP/2, and energy values are also slightly different.)

In the present work, we performed six multicanonical Monte Carlo simulations of 1 000 000 Monte Carlo sweeps each, where one Monte Carlo sweep updates all torsion angles in the peptide once. The six runs are: one run each with $\epsilon = 2$ and $\epsilon =$ sig for the three peptides. The simulations were started from random initial conformations.

The criterion we adopt for α-helix formation is as follows: We consider that a residue is in the α-helix configuration when the dihedral angles (ϕ,ψ) fall in the range ($-70 \pm 30°$, $-37 \pm 30°$). The length l of a helical segment is then defined by the number of successive residues which are in the α-helix configuration. The number n of helical residues in a conformation is defined by the sum of l over all helical segments in the conformation. Note that we have $n \geq l$ with the equality holding when there exists just one (or no) helical segment in the conformation.

Results and Discussion

We first examine how much of the configuration space the multicanonical simulations explore. As explained in the Methods section, a simulation in the multicanonical ensemble performs a one-dimensional random walk in the potential energy space. It should visit not only the ground-state regime but also states with very high energy. This ensures that the simulations avoid getting trapped in configurations with energy local minima. Since configurations are sampled over a large range of energies, the reweighting techniques allow one to calculate thermodynamic quantities as functions of temperature for a wide range of temperatures. As an example, we display in Figure 1a the "time series" of the total potential energy E_{tot} (in eq 4) for Peptide II with the sigmoidal dielectric function ($\epsilon =$ sig). The

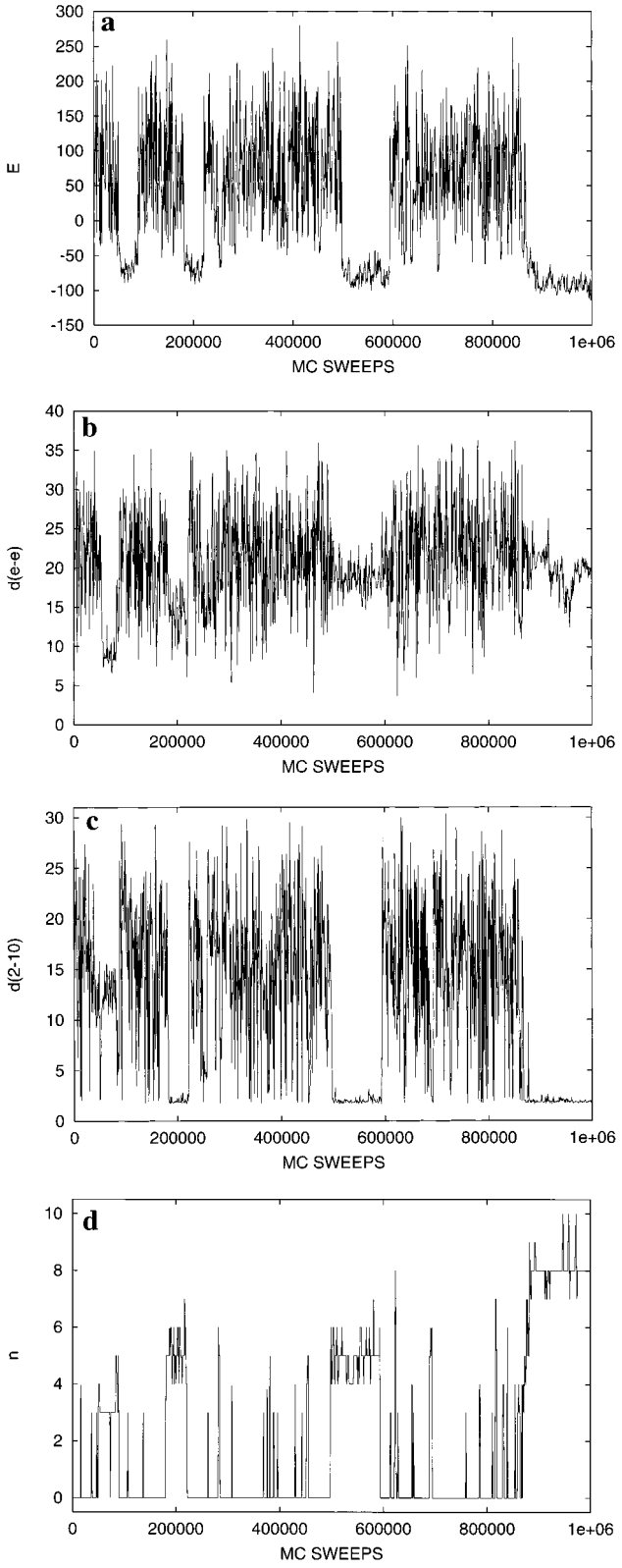

Figure 1. Time series of the total potential energy E_{tot} (kcal/mol) (a), the end-to-end distance d_{e-e} (Å) (b), the side-chain distance d_{2-10} (Å) between Glu-2 and Arg-10 (c), and the number of helical residues n (d) of Peptide II in the case of ϵ = sig obtained from a single multicanonical simulation of 1 000 000 MC sweeps.

results indeed exhibit a random walk in energy space covering a range of a few hundred kcal/mol. The random walk visits the low-energy regions at least four times. The more the number of independent excursions into the low-energy region is, the more reliable the calculated thermodynamic quantities at low

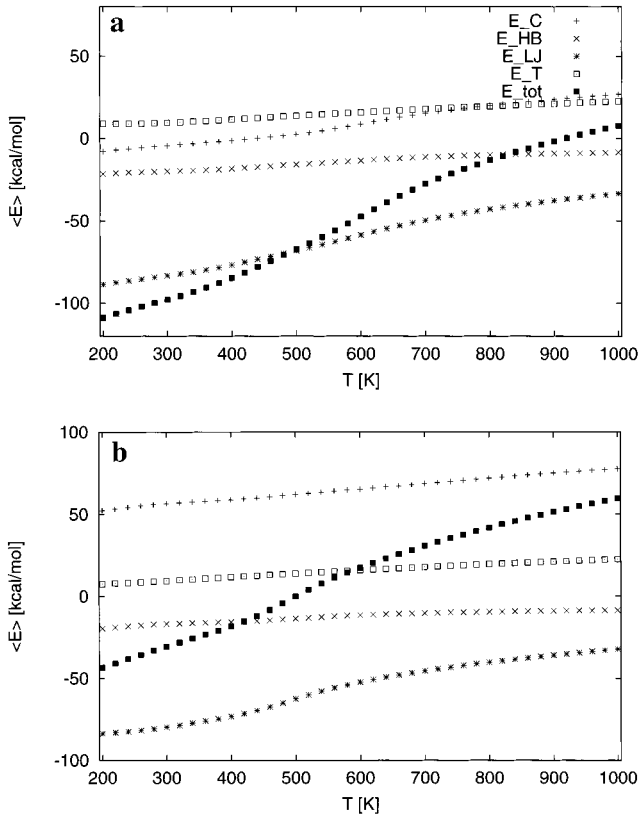

Figure 2. Average potential energies $\langle E \rangle_T$ (kcal/mol) of Peptide II as a function of temperature T (K) in the cases ϵ = sig (a) and $\epsilon = 2$ (b). They were obtained from a single multicanonical simulation of 1 000 000 MC sweeps for each case.

temperatures are. The random walk in energy space naturally causes random walks of other quantities. For instance, we show in Figure 1b−d the corresponding time series of the end-to-end distance d_{e-e}, side-chain distance d_{2-10} between Glu-2 and Arg-10, and number of helical residues n. Here, the end-to-end distance d_{e-e} is defined to be the distance between N of Lys-1 and O of Met-13 and is a measure for the compactness of a conformation. The distance d_{2-10} is defined to be the smallest of the distance between O^{ϵ} in the side chain of Glu-2 and H^{η} in the side chain of Arg-10 and is introduced in order to monitor the formation of the characteristic salt bridge between the side chains of Glu-2 and Arg-10, which is known to exist both in the NMR experiment[2] and in the X-ray experiment.[3] Finally, the number of helical residues n is a measure for the helicity of a conformation. Comparing Figure 1a and Figure 1b−d, we clearly observe correlations and anticorrelations of the behaviors: As the energy E_{tot} is decreased, both d_{e-e} and d_{2-10} tend to decrease, while the number of helical residues n tends to increase. Especially, the correlation between E_{tot} and d_{2-10} is conspicuous, indicating that for Peptide II this characteristic salt bridge is formed at low energies. We will further discuss the salt bridge formations below.

As emphasized above, the results from a single simulation run in multicanonical ensemble can be used to calculate various thermodynamic quantities as functions of temperature for a wide range of temperatures (see eq 3). The first example of such calculations we show here is average potential energy as a function of temperature. In Figure 2a we plot the average total potential energy and each component (in eq 4) for the case of Peptide II with ϵ = sig. The corresponding plot for Peptide II with $\epsilon = 2$ is shown in Figure 2b. One commonly observed point in both figures which holds also for the other peptides

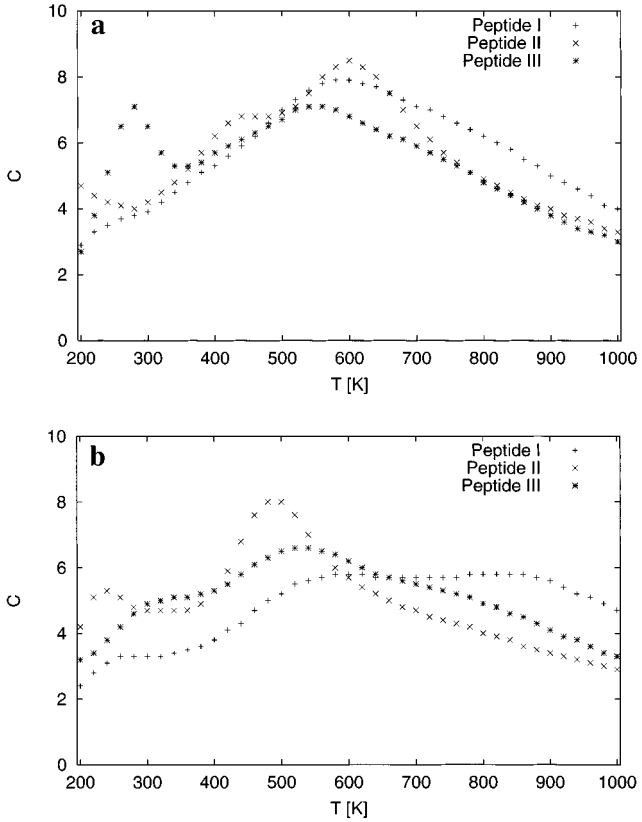

Figure 3. Specific heat C of the three peptides as a function of temperature T (K) in the cases $\epsilon = \text{sig}$ (a) and $\epsilon = 2$ (b). Each result was obtained from a single multicanonical simulation of 1 000 000 MC sweeps.

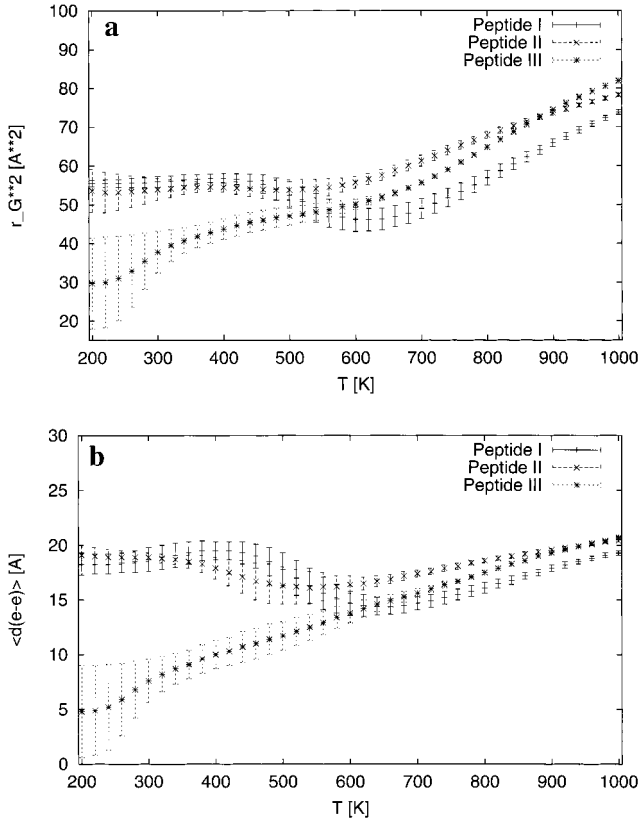

Figure 4. Radius of gyration r_G^2 (Å^2) (a) and end-to-end distance d_{e-e} (Å) (b) of the three peptides as a function of temperature T (K) in the case $\epsilon = \text{sig}$. They were obtained from a single multicanonical simulation of 1 000 000 MC sweeps for each peptide.

(data not shown) is that among the component terms both electrostatic and Lennard-Jones terms vary most with the temperature. This is contrasted with our previous works on peptides with only electrically neutral side chains (Met-enkephalin[9] and homooligomers[11]), where the changes of the Lennard-Jones term dominate that of the total potential energy. Hence, we understand that when some of the side chains are charged in the peptide, the contributions from the electrostatic interactions become a key factor in studying the peptide conformations (together with the Lennard-Jones term that is common in any peptide).

The fluctuation of the potential energy is the specific heat. Here, the quantity is defined by

$$C \equiv \frac{1}{Nk_B}\frac{\mathrm{d}(\langle E_{\mathrm{tot}}\rangle_T)}{\mathrm{d}T} = \beta^2 \frac{\langle E_{\mathrm{tot}}{}^2\rangle_T - \langle E_{\mathrm{tot}}\rangle_T{}^2}{N} \tag{6}$$

where N (=13) is the number of amino acid residues in the peptide. When given as a function of temperature, the peak of the specific heat indicates the presence of some transition of states. For instance, that for the case of Met-enkephalin implied the transition temperature of coil−globule phase transition,[21] while that for the case of polyalanine implied the transition temperature of helix−coil transitions.[11] In Figure 3 we show the specific heat as a function of temperature for the three peptides in two cases of dielectric functions. The peaks are located around $T = 500-600$ K for all cases. These peaks, however, are not as pronounced as in the cases for Met-enkephalin and polyalanine, and so there exists no clear phase-transition behavior this time. It seems that some of the data indicate the presence of more than one peak. However, this is not conclusive and should be checked carefully by simulations with more MC sweeps.

In the case of Met-enkephalin in the gas phase it was shown that the peak in the specific heat indicates a transition between a low-temperature phase dominated by compact structures and a high-temperature phase populated with extended coil configurations.[21] The situation is more complicated for C-peptide. We display in Figure 4a the radius of gyration r_G^2 and in Figure 4b the average end-to-end distance $\langle d_{e-e}\rangle_T$ as a function of temperature for the three peptides in the case for $\epsilon = \text{sig}$. Here, the radius of gyration r_G is defined by

$$r_G{}^2 = \left\langle \frac{1}{M}\sum_{i=1}^{M}\left|\vec{r}_i - \vec{r}_0\right|^2 \right\rangle_T \tag{7}$$

where M is the total number of atoms in the peptide and $\vec{r}_0$ is the "center of mass" coordinate vector:

$$\vec{r}_0 = \frac{1}{M}\sum_{i=1}^{M}\vec{r}_i \tag{8}$$

In both plots we observe that Peptides I and II have similar behavior. For both peptides, the radius of gyration stays more or less constant below $T \approx 500$ K, but increases fast above this temperature.

While the average end-to-end distance $\langle d_{e-e}\rangle_T$ for Met-enkephalin is a monotonically increasing function of temperature,[22] that for Peptides I and II has a minimum around $T = 500-600$ K, which is the temperature range where we have a peak in specific heat (see Figure 3). Above this temperature, $\langle d_{e-e}\rangle_T$ increases fast with temperature, but there is in addition also a small increase with decreasing temperature. This is presumably because longer α-helices are formed at lower

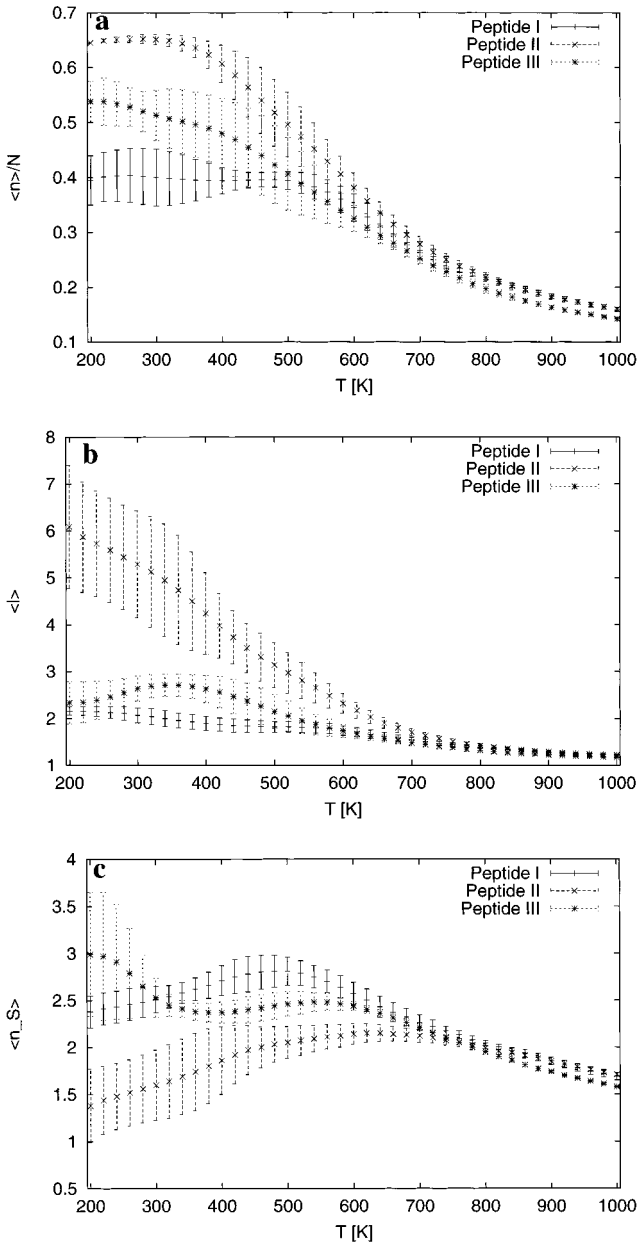

Figure 5. Average helicity $\langle n\rangle_T/N$ (a), average length $\langle l\rangle_T$ of a helical segment (b), and average number of helical segments $\langle n_S\rangle_T$ (c) of the three peptides as a function of temperature T (K) in the case ϵ = sig. They were obtained from a single multicanonical simulation of 1 000 000 MC sweeps for each peptide.

temperatures, which elongates the peptide. Hence, as discussed in detail below, we can also show that α-helices that existed at low temperatures cease to form in the temperature range T = 500−600 K. On the other hand, Peptide III shows a different behavior. Both r_G and $\langle d_{e-e}\rangle_T$ decrease monotonically with decreasing temperature, and the relation with the peak in specific heat is much less pronounced. In Peptides I and II, the side-chain repulsion between Lys-1^+ and His-12^+ tends to extend the peptide, while this repulsion does not exist for Peptide III, and we expect for this peptide more compact structures than for Peptides I and II.

We now examine how much α-helix formation was observed in the simulations. In Figure 5a we display the average helicity $\langle n\rangle_T/N$ (N = 13) as a function of temperature for the three peptides. Only the case for ϵ = sig is shown, since the other case (ϵ = 2) gives similar results. We observe the formation of α-helices at low temperatures in all three peptides. Peptide II

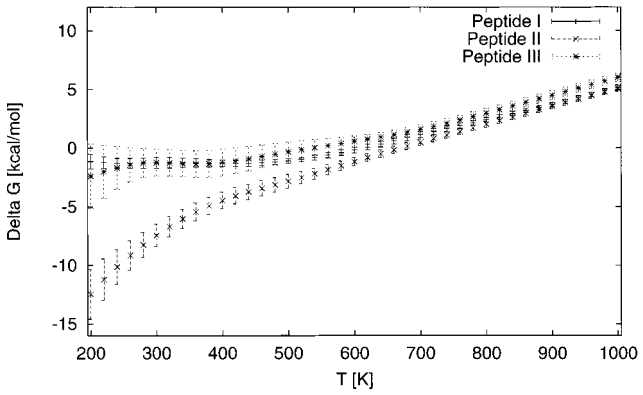

Figure 6. Free energy difference $\Delta G = G_H - G_{NH}$ (kcal/mol) between helix (H) and nonhelix (NH) states of the three peptides as a function of temperature T (K) in the case ϵ = sig. They were obtained from a single multicanonical simulation of 1 000 000 MC sweeps for each peptide.

is the most helix-forming among the three, then Peptide III, and finally Peptide I is the least helix-forming. We also observe that the helix−coil transitions take place around T = 500−600 K. This fact suggests that the peaks in the specific heat in Figure 3 around this temperature range indeed imply the existence of helix−coil transition (especially the transition is most obvious for Peptide II).

The helix−coil transition temperatures we obtained here are similar for ϵ = 2 and ϵ = sig, and too high compared to the experimental results.[1,2] However, it is known that the transition temperatures calculated from simulations in the gas phase tend to be significantly higher than those from simulations with solvent. For instance, the helix−coil transition temperature of a homooligomer of 10 alanine residues in gas phase is calculated to be about 400−450 K,[9] while preliminary simulations of the same homooligomer in aqueous solution gives the value around 300−350 K.[23] This implies that our representation of solvent effects by the sigmoidal dielectric function (ϵ = sig) is not accurate enough to give the precise value of the helix-coil transition temperature despite the good agreement in other quantities.

The average length $\langle l\rangle_T$ of a helical segment and the average number of helical segments $\langle n_S\rangle_T$ as a function of temperature for the corresponding cases are depicted in Figure 5b and Figure 5c, respectively. These figures show that there is a remarkable difference between Peptide II and Peptides I and III. Both the average length $\langle l\rangle_T$ of a helical segment and the average number of helical segments $\langle n_S\rangle_T$ differ little between Peptides I and III and indicate that while the helical content for the two peptides is as high as 40−50% (Figure 5a), they form several short helical segments rather than a single, long helix as in the case of Peptide II. This explains also why Peptide III has such a small end-to-end distance (Figure 4b), while it has a relatively high helical content (Figure 5a). The facts that there is a clear difference in helicity between Peptide II and Peptides I and III and that there is little difference in helicity between Peptide I and Peptide III seem to indicate that the most important charge effect in the present study is caused by that of the side chain of Glu-9: This charge hinders the formation of a long α-helix in C-peptide. Although the previous work by Monte Carlo simulated annealing for ϵ = 2 case[4] confirmed the experimental results[1,2] which imply that charges of Glu-2 and His-12 are necessary for α-helix stability (Peptide III versus Peptide I) and that more helix stability is obtained if the charge of Glu-9 is removed (Peptide II versus Peptide I), the more quantitative analyses of the present work seem to confirm only the latter point. The helix−coil

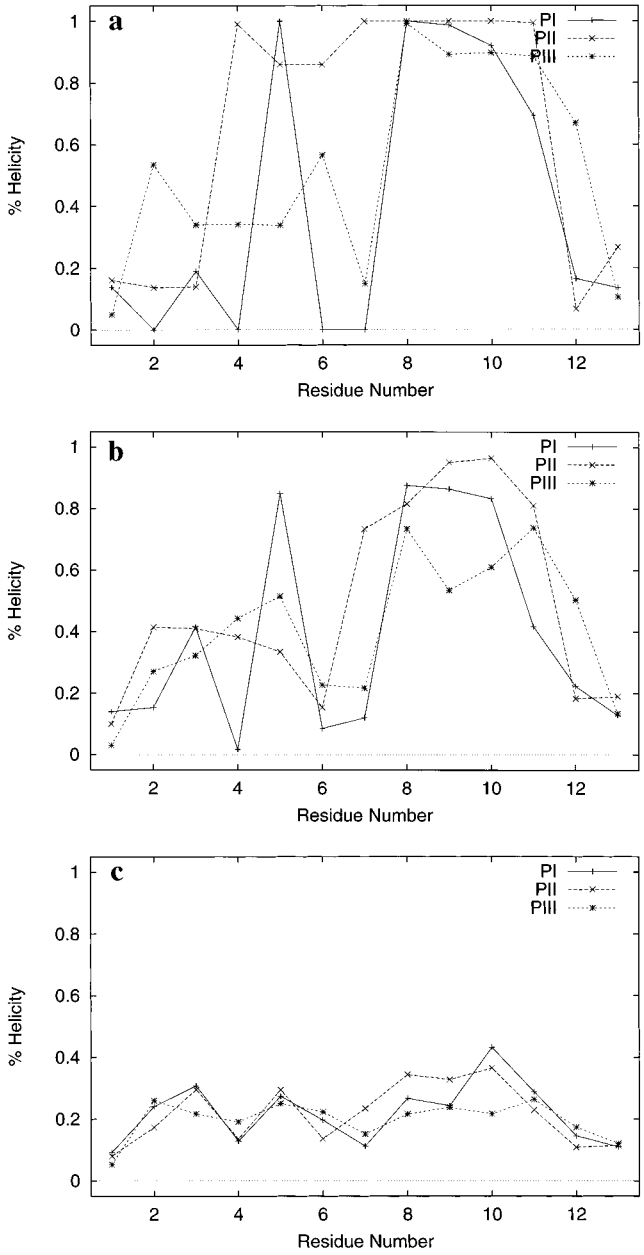

Figure 7. Average % helicity of the three peptides as a function of residue number at $T = 273$ K (a), $T = 500$ K (b), and $T = 800$ K (c) in the case $\epsilon =$ sig. Here, symbols PI, PII, and PIII stand for Peptide I, Peptide II, and Peptide III, respectively. Each result was obtained from a multicanonical simulation of 1 000 000 MC sweeps.

transition can be further studied by calculating the free energy differences $\Delta G \equiv G_H - G_{NH}$ between helix (H) and nonhelix (NH) states. Here, a conformation is considered to be in the helix state if it has a segment with helix length $l \geq 3$. (Note that $l = 3$ corresponds to roughly one turn of α-helix.) The free energy differences were calculated from

$$\Delta G(T) = -RT \ln \frac{\langle N_{\mathrm{H}} \rangle_T}{\langle N_{\mathrm{NH}} \rangle_T} \tag{9}$$

where R is the gas constant, and $\langle N_H \rangle_T$ and $\langle N_{NH} \rangle_T$ are the average numbers of conformations at temperature T in helix state and in nonhelix state, respectively. In Figure 6 we display ΔG as a function of temperature. Only the case for $\epsilon =$ sig is shown, since the other case ($\epsilon = 2$) gives similar results. Again we observe that Peptides I and III differ from Peptide II. For

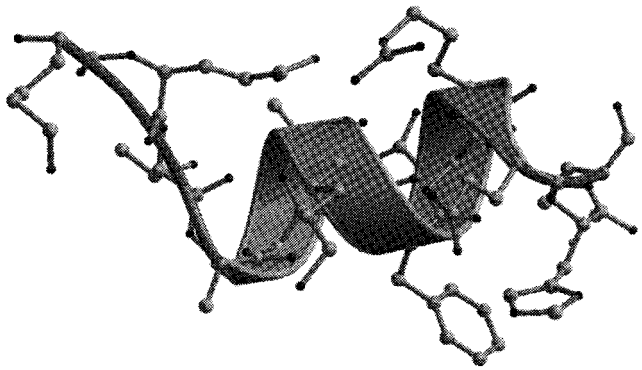

Figure 8. Conformation of C-peptide deduced from the X-ray crystallographic experiments of ribonuclease A (Brookhaven Protein Data Bank file 8RAT).[3] The figure was created with Molscript[24] and Raster3D.[25]

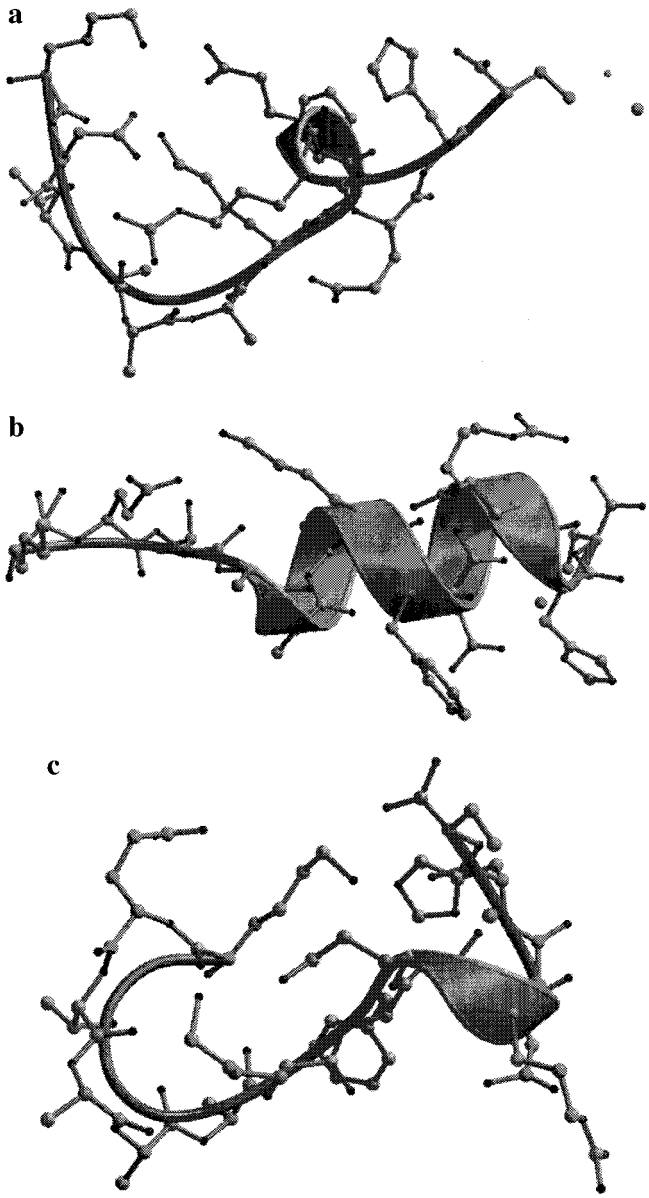

Figure 9. Lowest-energy conformations of Peptide I (a), Peptide II (b), and Peptide III (c) obtained during a multicanonical simulation of 1 000 000 MC sweeps in the case $\epsilon = 2$. The figures were created with Molscript[24] and Raster3D.[25]

Peptide II helical states are strongly favored below $T = 500-600$ K, while for Peptides I and III the free energy preference

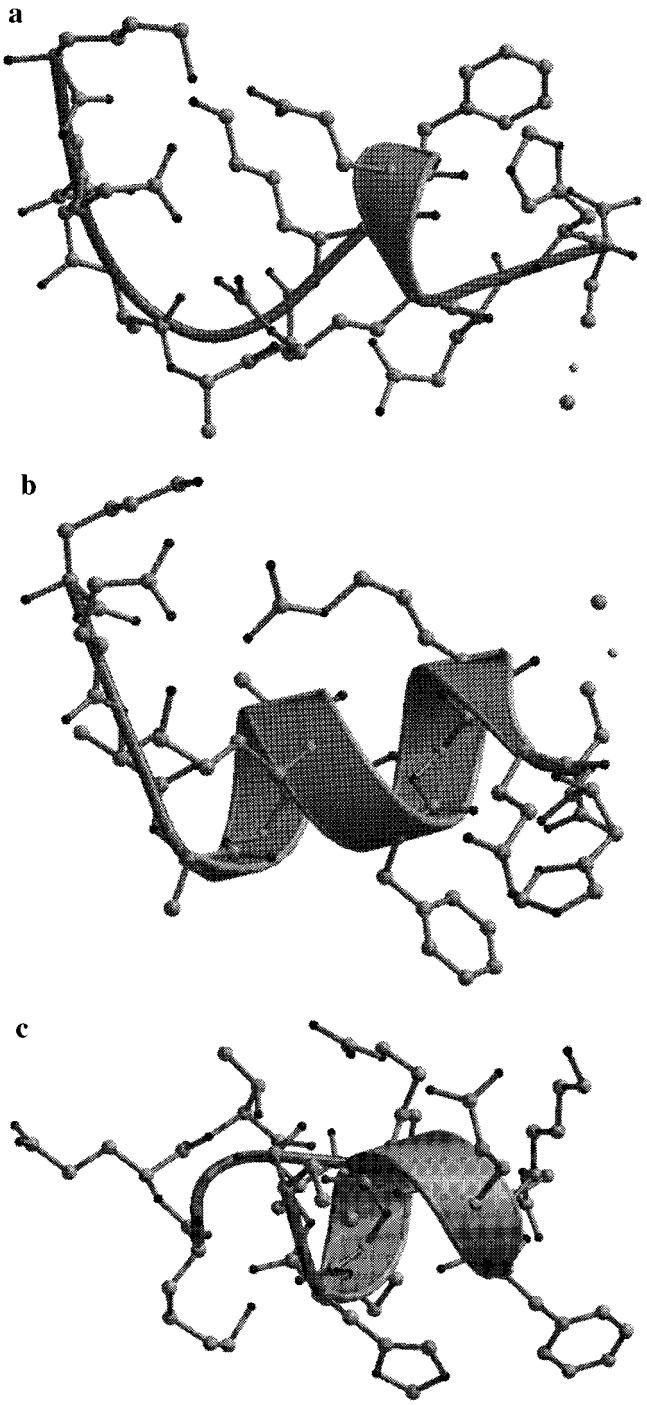

Figure 10. Lowest-energy conformations of Peptide I (a), Peptide II (b), and Peptide III (c) obtained during a multicanonical simulation of 1 000 000 MC sweeps in the case ϵ = sig. The figures were created with Molscript[24] and Raster3D.[25]

of helical conformations is much less pronounced. This result again supports the hypothesis that it is the side-chain charge of Glu-9 that is mainly responsible for the hindrance of α-helix formation.

The structure of the segment corresponding to the C-peptide that is obtained from X-ray diffraction experiments[3] of entire ribonuclease A has an α-helix from Ala-4 to Gln-11. The same data also indicate the existence of a salt bridge between Glu-2^- and Arg-10^+. Furthermore, the NMR experiments at $T \approx$ 273 K established the presence of this salt bridge in an isolated C-peptide analogue.[2] These data also suggested that the N-terminus of the peptide is less helical than the remainder of the peptide and it was claimed that this reduction of helicity near the N-terminus arises from the formation of the characteristic salt bridge between Glu-2^- and Arg-10^+.[2] In order to study whether our simulation results agree with these experimental facts, we calculated the average % helicity as a function of the residue number at three temperatures (273, 500, and 800 K). The results for the three peptides in the case of ϵ = sig are shown in Figure 7. At T = 273 K one finds that the residues are successively helical from Phe-8 to Gln-11, from Ala-4 to Gln-11, and from Phe-8 to Gln-11 for Peptides I, II, and III, respectively. Hence, the results for Peptide II are the closest to those of the X-ray experiments. At T = 500 K the α-helix toward the C-terminus remains for the three peptides. This means that for Peptide II the helicity is reduced drastically for residues from Ala-4 to Ala-6. At T = 800 K the helicity for the three peptides is small for all residues because of the increased thermal fluctuations. The results for the case of ϵ = 2 are similar (data not shown), but for Peptide II the helicity is slightly less in the residues from Ala-5 to Lys-7 than in the case for ϵ = sig. Hence, it seems that the simulation results for Peptide II in the case for ϵ = sig agree most with those of the above experiments. Since the characteristic salt bridge between Glu-2 and Arg-10 does not exist for Peptide III (see below), these peptide analogues seem to have intrinsic tendency to form less α-helix in the N-terminus region regardless of whether this salt bridge exists or not.

We now compare the lowest-energy conformations obtained by the present simulations and the structure deduced from the X-ray experiments.[3] Figure 8 depicts the conformation obtained from the X-ray experiments, while Figures 9 and 10 show the lowest-energy conformations obtained from the simulations for the cases of ϵ = 2 and ϵ = sig, respectively. In Table 2 we

TABLE 2: α-Helix Content and Salt Bridge Formations in the Lowest-Energy Conformations Obtained by the Present Simulations Together with the Conformation Deduced from the X-ray Experiments

conformation	α-helix	salt bridge
X-ray	Ala-4 to Gln-11	Glu-2 and Arg-10
Peptide I (ϵ = 2)	Phe-8 to Arg-10	Lys-1 and Glu9, Glu-2 and Lys-7, Glu-2 and Arg-10
Peptide II (ϵ = 2)	Ala-4 to His-12	Glu-2 and Lys-7
Peptide III (ϵ =2)	Glu-9 to Gln-11	Lys-1 and Glu9
Peptide I (ϵ = sig)	Phe-8 to Arg-10	Lys-1 and Glu9, Glu-2 and Lys-7, Glu-2 and Arg-10
Peptide II (ϵ = sig)	Ala-4 to Gln-11	Glu-2 and Lys-7, Glu-2 and Arg-10
Peptide III (ϵ = sig)	Phe-8 to His-12	

TABLE 3: Root-Mean-Square Distances (Å) between Pairs of Conformations[a]

	0	1	2	3	4	5	6[b]
0		3.6	3.2	1.9	1.4	4.5	5.2
1	5.2		2.5	4.0	3.8	3.7	5.1
2	5.3	3.0		3.6	3.1	4.0	5.3
3	3.5	5.8	5.6		2.6	5.0	5.9
4	2.7	4.7	4.8	4.1		4.4	5.2
5	6.4	5.2	5.6	6.3	6.0		4.7
6	6.1	6.5	6.7	6.6	6.0	7.0	

[a] The rms distances were calculated with respect to non-hydrogen atoms only. The upper-right triangular section is the results for atoms in the backbone only, and the lower-left triangular section is the results with all non-hydrogen atoms taken into account. [b] Conformation 0 is the structure obtained from the X-ray experiments (Brookhaven Protein Data Bank file 8RAT).[3] Conformations 1 and 2 are the lowest-energy conformations of Peptide I in the cases for ϵ = 2 and ϵ = sig, respectively. Conformations 3 and 4 are corresponding conformations of Peptide II, and conformations 5 and 6 are those of Peptide III.

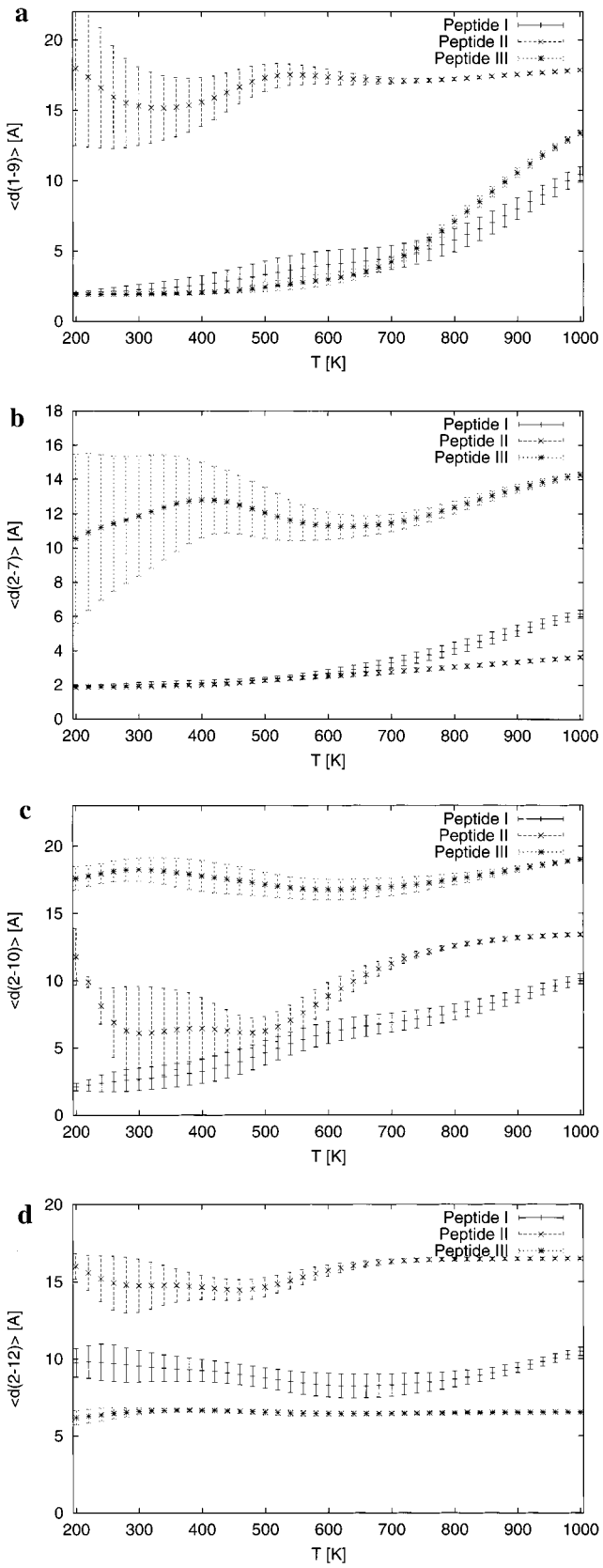

Figure 11. Average distances between a pair of side chains $\langle d_{1-9}\rangle_T$ (Å) (a), $\langle d_{2-7}\rangle_T$ (Å) (b), $\langle d_{2-10}\rangle_T$ (Å) (c), and $\langle d_{2-12}\rangle_T$ (Å) (d) of the three peptides as a function of temperature T (K) in the case $\epsilon = 2$. They were obtained from a single multicanonical simulation of 1 000 000 MC sweeps for each peptide.

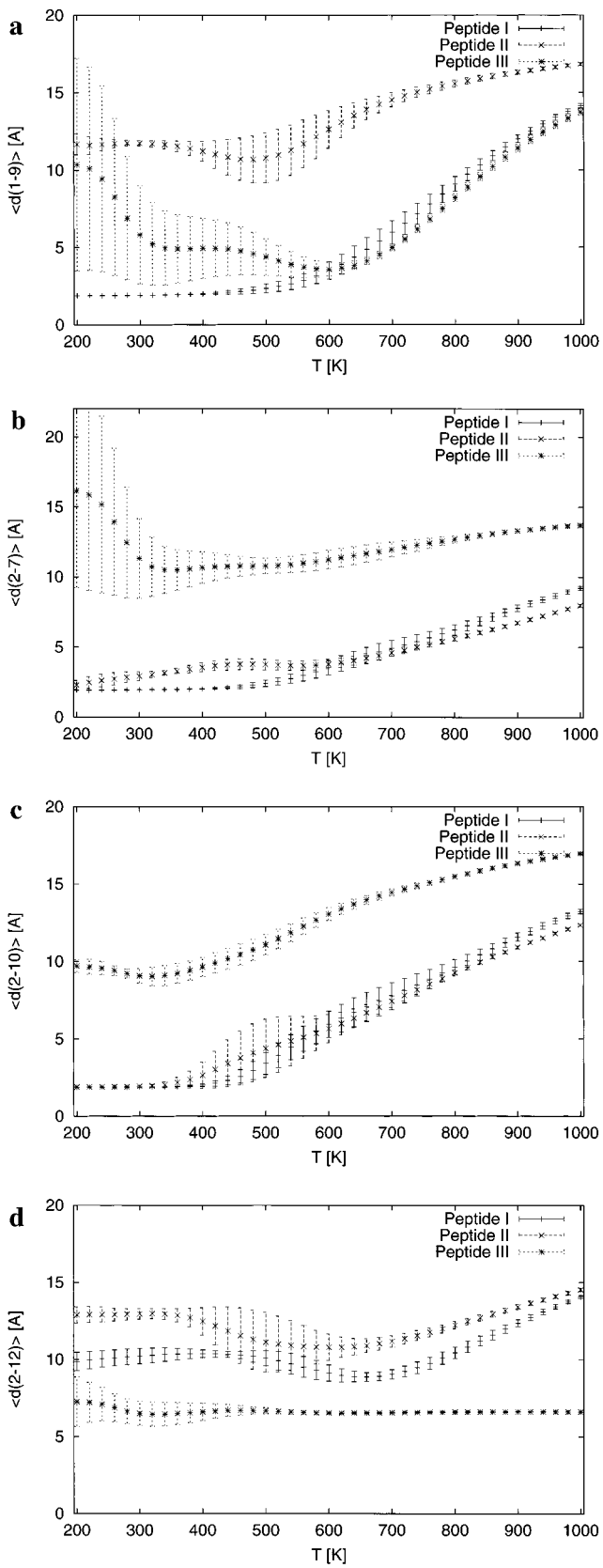

Figure 12. Average distances between a pair of side chains $\langle d_{1-9}\rangle_T$ (Å) (a), $\langle d_{2-7}\rangle_T$ (Å) (b), $\langle d_{2-10}\rangle_T$ (Å) (c), and $\langle d_{2-12}\rangle_T$ (Å) (d) of the three peptides as a function of temperature T (K) in the case $\epsilon =$ sig. They were obtained from a single multicanonical simulation of 1 000 000 MC sweeps for each peptide.

summarize the α-helix content and salt bridge formations in these structures. We observe that for both cases ($\epsilon = 2$ and $\epsilon =$ sig) the lowest-energy conformations for Peptide II have the most similar backbone structures to that from the X-ray

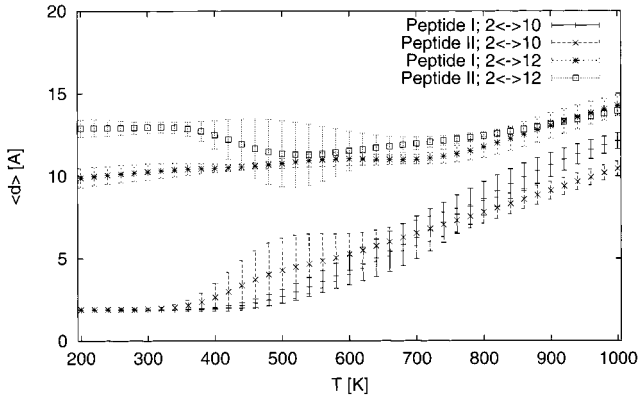

Figure 13. Average distances between a pair of side chains $\langle d_{2-10}\rangle_T$ (Å) and $\langle d_{2-12}\rangle_T$ (Å) of Peptides I and II as a function of temperature T (K) in the case ϵ = sig. They were obtained from a single multicanonical simulation of 1 000 000 MC sweeps for each peptide, and the averages were taken only over helical conformations.

experiments. In particular, as shown in Table 2, the lowest-energy conformation of Peptide II for ϵ = sig (Figure 10b) has an α-helix from Ala-4 to Gln-11 in remarkable agreement with the corresponding structure deduced from the X-ray experiments (Figure 8). Note also that for Peptide II the characteristic salt bridge between Glu-2 and Arg-10 is observed only in the case of ϵ = sig, i.e., only when some solvation effects are included.

The structure comparisons can be made more quantitative by calculating the root-mean-square distances (rmsd) among the seven conformations. The results are listed in Table 3. As is clear from the table, the lowest-energy conformation of Peptide II in the case of ϵ = sig resembles most the structure from the X-ray experiments (rmsd = 1.4 Å for the backbone structure and 2.7 Å when all non-hydrogen atoms are taken into account). We also observe that the differences in structures are in general smaller between the cases $\epsilon = 2$ and ϵ = sig than those among the three peptides.

The formation of salt bridges can be studied by calculating the average distance $\langle d_{i-j}\rangle_T$ between a pair of charged side chains i and j at a low temperature T. We have investigated four pairs, 1−9, 2−7, 2−10, and 2−12. Here, the distance between the side-chain pair Glu-2−Arg-10, for instance, is defined to be the smallest of the distance between O^{ϵ} of the side chain of Glu-2 and H^{η} of the side chain of Arg-10. Other distances are defined in a similar manner. The average distances $\langle d_{i-j}\rangle_T$ as a function of temperature are given in Figure 11 and Figure 12 in the cases of $\epsilon = 2$ and ϵ = sig, respectively. It is obvious from the figures that if a side chain is uncharged, salt bridges are not formed. For example, the salt bridge between Lys-1 and Glu-9 does not exist for Peptide II, since Glu-9 is neutral in Peptide II (see Figure 12a). Interesting cases are when even a charged side-chain pair does not form a salt bridge. For instance, for Peptides I and II the side-chain charges would allow a salt bridge between Glu-2^- and His-12^+. However, the results of our simulations suggest that this salt bridge is not formed. The nonformation of the salt bridge between Glu-2 and His-12 can be understood easily because the pair of the residues is far apart along the main chain.

In Figure 13 we display the average distances $\langle d_{2-10}\rangle_T$ and $\langle d_{2-12}\rangle_T$ as a function of temperature for Peptides I and II in the case ϵ = sig, where the averages are taken only over helical conformations. It is obvious that there is for both peptides a strong correlation between the helicity and the Glu-2^- and Arg-10^+ salt bridge, and a strong anticorrelation with a salt bridge between Glu-2^- and His-12^+. Helical conformations with the salt bridge between Glu-2 and Arg-10 are energetically more favored over nonhelical structures than without this salt bridge. For Peptide I (and ϵ = sig) the enthalpy difference ΔH at T = 273 K between helical and nonhelical conformers is ΔH = −1.5(3) kcal/mol with the salt bridge between Glu-2 and Arg-10, and ΔH = −0.2(3.2) kcal/mol when this salt bridge does not exist. For Peptide II we find ΔH = −19 (5) kcal/mol with the salt bridge and ΔH = −13(7) kcal/mol without the salt bridge. Note that while the salt bridge between Glu-2 and Arg-10 helps to stabilize the helix, it seems not to be the dominant effect; comparing the enthalpy difference ΔH between helix and nonhelix states for Peptides I and II, we see that removing the side-chain charge of Glu-9 increases ΔH more than the formation of the salt bridge does.

Conclusions

In this article, we have presented the results of multicanonical Monte Carlo simulations applied to study the α-helix stability of C-peptide of ribonuclease A. The results were in good qualitative agreement with various implications of CD, NMR, and X-ray experiments. We demonstrated that the side-chain charges play an important role in the helix stability. In particular, the charge of residue Glu-9 seems to hinder the formation of a long helix, while the charges of the side-chain pair Glu-2 and Arg-10 allow a salt bridge between these two residues which stabilizes the α-helix. It should be emphasized that the simulations were performed from completely random initial conformations and that no structural information from experiments was used as input.

Acknowledgment. Our simulations were performed on computers in the Computer Center of the Institute for Molecular Science (IMS), Okazaki, Japan. This work is supported by a Grant-in-Aid for Scientific Research from the Japanese Ministry of Education, Science, Sports and Culture.

References and Notes

(1) Shoemaker, K. R.; Kim, P. S.; Brems, D. N.; Marqusee, S.; York, E. J.; Chaiken, I. M.; Stewart, J. M.; Baldwin, R. L. *Proc. Natl. Acad. Sci. U.S.A.* **1985**, *82*, 2349−2353.

(2) Osterhout, J. J.; Baldwin, R. L.; York, E. J.; Stewart, J. M.; Dyson, H. J.; Wright, P. E. *Biochemistry* **1989**, *28*, 7059−7064.

(3) Tilton, R. F., Jr.; Dewan, J. C.; Petsko, G. A. *Biochemistry* **1992**, *31*, 2469−2481.

(4) (a) Kawai, H.; Okamoto, Y.; Fukugita, M.; Nakazawa, T.; Kikuchi, T. *Chem. Lett.* **1991**, 213−216. (b) Okamoto, Y.; Fukugita, M.; Nakazawa, T.; Kawai, H. *Protein Eng.* **1991**, *4*, 639−647.

(5) Kirkpatrick, S.; Gelatt, C. D., Jr.; Vecchi, M. P. *Science* **1983**, *220*, 671−680.

(6) Berg, B. A.; Neuhaus, T. *Phys. Lett.* **1991**, *B267*, 249−253.

(7) Berg, B. A. *Int. J. Mod. Phys.* **1992**, *C3*, 1083−1096.

(8) Hansmann, U. H. E.; Okamoto, Y. *J. Comput. Chem.* **1997**, *18*, 920−933.

(9) Hansmann, U. H. E.; Okamoto, Y. *J. Comput. Chem.* **1993**, *14*, 1333−1338.

(10) (a) Hansmann, U. H. E.; Okamoto, Y. *J. Phys. Soc. Jpn.* **1994**, *63*, 3945−3949. (b) Hansmann, U. H. E.; Okamoto, Y. *Physica A* **1994**, *212*, 415−437.

(11) (a) Okamoto, Y.; Hansmann, U. H. E.; Nakazawa, T. *Chem. Lett.* **1995**, 391−392. (b) Okamoto, Y.; Hansmann, U. H. E. *J. Phys. Chem.* **1995**, *99*, 11276−11287.

(12) Hansmann, U. H. E.; Okamoto, Y. *J. Phys. Chem.* **1998**, *B102*, 653−656.

(13) Metropolis, N.; Rosenbluth, A. W.; Rosenbluth, M. N.; Teller, A. H.; Teller, E. *J. Chem. Phys.* **1953**, *21*, 1087−1092.

(14) Ferrenberg, A. M.; Swendsen, R. H. *Phys. Rev. Lett.* **1988**, *61*, 2635−2638; *Phys. Rev. Lett.* **1989**, *63*, 1658−1658(E), and references given in the erratum.

(15) Ihara, S.; Ooi, T.; Takahashi, S. *Biopolymers* **1982**, *21*, 131−145.

(16) Shoemaker, K. R.; Kim, P. S.; York, E. J.; Stewart, J. M.; Baldwin, R. L. *Nature* **1987**, *326*, 563−567.

(17) (a) Momany, F. A.; McGuire, R. F.; Burgess, A. W.; Scheraga, H. A. *J. Phys. Chem.* **1975**, *79*, 2361−2381. (b) Némethy, G.; Pottle, M. S.; Scheraga, H. A. *J. Phys. Chem.* **1983**, *87*, 1883−1887. (c) Sippl, M. J.; Némethy, G.; Scheraga, H. A. *J. Phys. Chem.* **1984**, *88*, 6231−6233.

(18) (a) Hingerty, B. E.; Ritchie, R. H.; Ferrell, T.; Turner, J. E. *Biopolymers* **1985**, *24*, 427−439. (b) Ramstein, J.; Lavery, R. *Proc. Natl. Acad. Sci. U.S.A.* **1988**, *85*, 7231−7235.

(19) Okamoto, Y. *Biopolymers* **1994**, *34*, 529−539.

(20) Daggett, V.; Kollman, P. A.; Kuntz, I. D. *Biopolymers* **1991**, *31*, 285−304.

(21) Hansmann, U. H. E.; Masuya, M.; Okamoto, Y. *Proc. Natl. Acad. Sci. U.S.A.* **1997**, *94*, 10652−10656.

(22) Hansmann, U. H. E.; Okamoto, Y.; Eisenmenger, F. *Chem. Phys. Lett.* **1996**, *259*, 321−330.

(23) Mitsutake, A.; Okamoto, Y., manuscript in preparation.

(24) Kraulis, P. J. *J. Appl. Crystallogr.* **1991**, *24*, 946−950.

(25) (a) Bacon, D.; Anderson, W. F. *J. Mol. Graphics* **1988**, *6*, 219−220. (b) Merritt, E. A.; Murphy, M. E. P. *Acta Crystallogr.* **1994**, *D50*, 869−873.